

Ground-state structure of a bilayer Wigner crystal with repulsive dielectric images

LADISLAV ŠAMAJ^{1,2} and EMMANUEL TRIZAC¹

¹ *Université Paris-Sud, Laboratoire de Physique Théorique et Modèles Statistiques, UMR CNRS 8626 91405 Orsay, France, EU*

² *Institute of Physics, Slovak Academy of Sciences - Dúbravská cesta 9, 845 11 Bratislava, Slovakia, EU*

received 1 September 2012; accepted in final form 27 October 2012
published online 10 December 2012

PACS 64.70.kp – Ionic crystals
PACS 68.65.Ac – Multilayers
PACS 73.20.-r – Electron states at surfaces and interfaces

Abstract – We study the ground-state structures of identical classical point charges with Coulomb interactions, confined between two symmetric parallel charged walls. For the well-understood homogeneous dielectric case with no electrostatic images, the charges evenly condense on the opposite walls, thereby forming a bilayer Wigner crystal; five structures compete upon changing the inter-wall separation. Here, we consider a dielectric jump between the walls and a solvent in which charges are immersed, implying repulsive images. Using recently developed series representations of lattice sums for Coulomb law, we derive the complete phase diagram. In contrast to the homogeneous dielectric case, the particles remain in a hexagonal Wigner monolayer up to a certain distance between the walls. Beyond this distance, a bifurcation occurs to a sequence of Wigner bilayers, each layer having a nonzero spacing from the nearest wall. Another new phenomenon is that the ground-state energy as a function of the wall separation exhibits a global minimum.

Copyright © EPLA, 2012

Introduction. – Bilayer Wigner crystals of electrons appear in various experimental settings: GaAs quantum wells [1,2] or other semiconductors [3], quantum dots [4], dusty plasmas [5], colloids [6], etc. Theoretically, it is relevant and nontrivial to understand the ground-state features of Coulombic bilayers, starting with the classical limit. This subject in its homogeneous dielectric version has received significant attention in the last few years, as such [7–12] or within more general finite temperature analysis [13–16].

We consider the ground state of an ensemble of (say elementary) classical point charges e , interacting through the $1/r$ usual Coulomb pair potential. The charges are confined between two symmetric parallel walls at distance d , carrying a uniform surface charge of density $-\sigma e$ (see fig. 1). The system as a whole is electroneutral. The static dielectric constant of the walls ε' can be, in general, different from the constant ε of the solvent in which the charges are immersed. The dielectric jump between the two moieties is defined as $\Delta = (\varepsilon - \varepsilon')/(\varepsilon + \varepsilon')$, so that $\Delta \in [-1, 1]$. The interval $\Delta \in [-1, 0)$ corresponds to attractive and $\Delta \in (0, 1]$ to repulsive electrostatic image charges. In realistic systems, in particular those of biological interest,

the wall mimics the interior of a polarizable colloid with $\varepsilon' \leq 10$ while $\varepsilon \simeq 80$ for water solvent, so Δ is close to 1.

In the well-understood homogeneous dielectric case $\Delta = 0$, Earnshaw theorem [17] tells us that in the ground state, the charges evenly condense on the opposite walls. The structure of the formed bilayer depends on a single dimensionless parameter $\eta = d\sqrt{\sigma}$. For $\eta = 0$, a genuine hexagonal Wigner crystal (structure I) is stable (provides the true minimum of the energy); this structure becomes unstable for an arbitrary small $\eta > 0$ [11,18,19]. In the opposite limit $\eta \rightarrow \infty$, the two layers decouple and a hexagonal Wigner crystal is formed on each plate (structure V); to minimize the inter-layer repulsion, these two crystals adopt a staggered configuration. For intermediate values of η , three other structures are met, see fig. 2: a staggered rectangular lattice (structure II), a staggered square lattice (structure III) and a staggered rhombic lattice (structure IV) [9]. The transitions between structures (II and III) and (III and IV) are of second order with mean-field critical indices [18,19]. The transition between structures (IV and V) is discontinuous, characterized by a skip of the angle φ to $\pi/3$ and by a mutual shift of the lattices on the opposite surfaces.

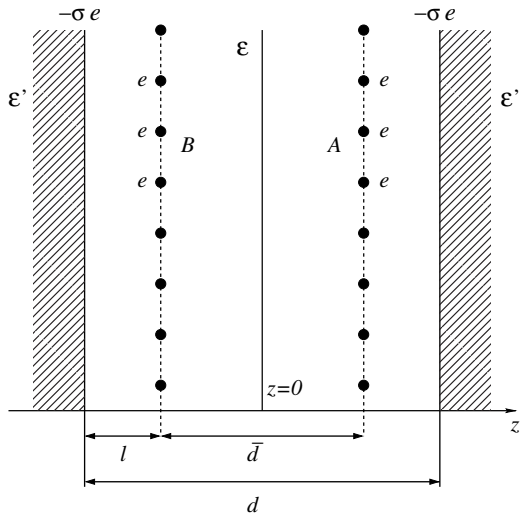


Fig. 1: The geometry of two dielectric walls at distance d , carrying the surface charge density $-\sigma e$. The particles of charge e form a Wigner bilayer which consists of two sub-lattices A and B at distance \bar{d} ; a monolayer corresponds to $\bar{d}=0$. The distance of each sub-lattice to the nearest wall is $l = (d - \bar{d})/2$.

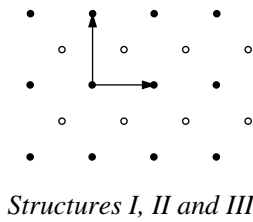


Fig. 2: Schematic representation of the different ground states encountered when the dimensionless distance η increases, in the homogeneous dielectric case $\Delta=0$. The open and filled symbols show the locations of ions on the opposite surfaces. The arrows are for the lattice vectors \mathbf{a}_1 and \mathbf{a}_2 , from which we define the aspect ratio $\delta = |\mathbf{a}_2|/|\mathbf{a}_1|$: $\delta = \sqrt{3}$ for structure I, $\delta = 1$ for structure III, while structure II is intermediate, having $1 < \delta < \sqrt{3}$. For structure IV, the order parameter is the angle φ between \mathbf{a}_1 and \mathbf{a}_2 . Structures IV and V have $\delta = 1$.

In this letter, we consider the dielectric jump $\Delta \in [0, 1]$, implying repulsive electrostatic image charges. The presence of repulsive image and self-image forces has intuitively two important effects on the ground state:

- the particles no longer collapse on the surface of the walls, but create a symmetric bilayer structure with a nonzero spacing from the walls, *i.e.* $\bar{d} \neq d$ in fig. 1;

- the intervals of η , inside which the structures I-V are stable, are changed. In particular, a monolayer with structure I is expected to be stable up to a critical value $\eta_{\text{I} \rightarrow \text{II}} > 0$ beyond which it bifurcates into a bilayer with structure II.

The nonzero spacing from the walls is confirmed in the limit $\eta \rightarrow \infty$ where the two layers decouple (up to a staggered shift) and each of them forms a neutral entity with the corresponding charged wall. For the resulting one-wall geometry, it was shown in ref. [20] that, as a result of balance between attractive surface charge and repulsive image charge forces, the stable hexagonal Wigner crystal of particles is formed at some distance l from the wall. This distance is given by $l = at/2$, where a is the lattice spacing of the two-dimensional Wigner crystal determined by the electroneutrality condition as $1 = (\sqrt{3}/2)a^2\sigma$ and the dimensionless parameter t is the solution of the transcendental equation

$$\sum_{j,k=-\infty}^{\infty} \frac{1}{(t^2 + j^2 + jk + k^2)^{3/2}} = \frac{4\pi}{\sqrt{3}} \frac{1 + \Delta}{\Delta} \frac{1}{t}. \quad (1)$$

The lattice sum on the lhs can be expressed as

$$\frac{2}{\pi} \int_0^{\infty} du \sqrt{u} e^{-ut^2} [\theta_3(e^{-u})\theta_3(e^{-3u}) + \theta_2(e^{-u})\theta_2(e^{-3u})], \quad (2)$$

where $\theta_2(q) = \sum_{n=-\infty}^{\infty} q^{(n-\frac{1}{2})^2}$ and $\theta_3(q) = \sum_{n=-\infty}^{\infty} q^{n^2}$ are the Jacobi theta functions with zero argument.

Method. – Our goal is to calculate the Coulomb interaction energy of the electroneutral system pictured in fig. 1. Each point will be represented by Cartesian coordinates as $\mathbf{r} = (\mathbf{R}, z)$, where $\mathbf{R} = (x, y)$ and the z -axis is perpendicular to the walls. The system is inhomogeneous along the z -axis, symmetric with respect to the $z=0$ plane. The wall surfaces, charged uniformly by $-\sigma e$, are localized at $z = \pm d/2$. The two Wigner sublayers, each formed of $N/2$ point charges e , are localized at $z = \bar{d}/2$ (sub-lattice A with sites $\{\mathbf{R}_j^A\}$) and at $z = -\bar{d}/2$ (sub-lattice B with sites $\{\mathbf{R}_j^B\}$). The distance of the Wigner sub-lattice A (respectively B) to the nearest wall at $z = +d/2$ (respectively $z = -d/2$) is $l = (d - \bar{d})/2$. We have $l > 0$ for the considered case with repulsive images $\Delta \in (0, 1]$ and $l = 0$ otherwise (for attractive images $\Delta \in [-1, 0)$, a small hard core around the particles is necessary to prevent thermodynamic collapse onto their images).

The Coulomb energy consists of three contributions:

- Particle-particle interactions:* The direct Coulomb potential between two points $\mathbf{r} = (\mathbf{R}, z)$ and $\mathbf{r}' = (\mathbf{R}', z')$, situated in between the walls, is given by

$$u_0(\mathbf{r}, \mathbf{r}') = \frac{1}{\epsilon} \frac{1}{\sqrt{|\mathbf{R} - \mathbf{R}'|^2 + (z - z')^2}}. \quad (3)$$

Due to the dielectric inhomogeneity, a unit charge at $\mathbf{r} = (\mathbf{R}, z)$ has an infinite number of electrostatic images

with the same vector \mathbf{R} [21]. The first sequence of images, generated by considering first the reflection with respect to the wall surface at $z = +d/2$, is localized at $(-1)^{n+1}(nd - z)$ with associated charges Δ^n ($n = 1, 2, \dots$). The second sequence, generated by considering first the reflection with respect to the wall surface at $z = -d/2$, is localized at $(-1)^n(nd + z)$ with associated charges Δ^n ($n = 1, 2, \dots$). The image Coulomb potential thus reads

$$u_{\text{im}}(\mathbf{r}, \mathbf{r}') = \frac{1}{\varepsilon} \sum_{n=1}^{\infty} \left\{ \frac{\Delta^{2n}}{\sqrt{|\mathbf{R} - \mathbf{R}'|^2 + (2nd + z - z')^2}} + \frac{\Delta^{2n}}{\sqrt{|\mathbf{R} - \mathbf{R}'|^2 + (2nd - z + z')^2}} + \frac{\Delta^{2n-1}}{\sqrt{|\mathbf{R} - \mathbf{R}'|^2 + [(2n-1)d + z + z']^2}} + \frac{\Delta^{2n-1}}{\sqrt{|\mathbf{R} - \mathbf{R}'|^2 + [(2n-1)d - z - z']^2}} \right\}. \quad (4)$$

The notation $u_{\text{im}}(\mathbf{r}, \mathbf{r}') \equiv u_{\text{im}}(|\mathbf{R} - \mathbf{R}'|; z, z')$ will be often used in what follows. The total energy of particles and their images is given by

$$E_{pp} = \frac{e^2}{2} \left[\sum_{j \neq k} u_0(\mathbf{r}_j, \mathbf{r}_k) + \sum_{j,k} u_{\text{im}}(\mathbf{r}_j, \mathbf{r}_k) \right]. \quad (5)$$

The term $j = k$ in the second sum corresponds to the interaction of particle j with its own image. Let us choose as a reference particle the one at site 1 of lattice A localized on the plane $z = \bar{d}/2$. The energy per particle is expressible as

$$\begin{aligned} \frac{E_{pp}}{N} = & \frac{e^2}{2\varepsilon} \left[\sum_{j \neq 1} \frac{1}{R_{1j}^{AA}} + \sum_j \frac{1}{\sqrt{(R_{1j}^{AB})^2 + \bar{d}^2}} \right] \\ & + \frac{e^2}{2} \left[u_{\text{im}}\left(0; \frac{\bar{d}}{2}, \frac{\bar{d}}{2}\right) + \sum_{j \neq 1} u_{\text{im}}\left(R_{1j}^{AA}; \frac{\bar{d}}{2}, \frac{\bar{d}}{2}\right) \right] \\ & + \sum_j u_{\text{im}}\left(R_{1j}^{AB}; \frac{\bar{d}}{2}, -\frac{\bar{d}}{2}\right). \end{aligned} \quad (6)$$

Here, $R_{1j}^{AA} \equiv |\mathbf{R}_1^A - \mathbf{R}_j^A|$ and similarly $R_{1j}^{AB} \equiv |\mathbf{R}_1^A - \mathbf{R}_j^B|$. Owing to the symmetry of the problem, the same formula holds if the reference particle sits on lattice B .

The lattice sums in the above expression have to be “regularized” by background terms in the following sense. Let us consider two plates at distance z , each of a large surface S . They carry the fixed surface charge density $-\sigma e$. At each plate, there are point charges e of surface density σ . The total number of particles $N = 2\sigma S$, so that the system as a whole is electroneutral. The dielectric constant is homogeneous, equal to ε . The

energy per unit surface due to the background-background interaction of the two $(-\sigma e)$ plates at distance z is given by $E_{bb}/S = -2\pi(\sigma e)^2 z/\varepsilon$. Equivalently, $E_{bb}/N = -\pi\sigma e^2 z/\varepsilon$. The interaction energy of charge e with $(-\sigma e)$ plate at distance z is $2\pi\sigma e^2 z/\varepsilon$. The total “background energy” per particle thus reads $\epsilon(z) = \pi\sigma e^2 z/\varepsilon$. Such term has to be added to and subtracted from each of the lattice sums in (6). The first term is unchanged, the second term becomes

$$\frac{e^2}{2\varepsilon} \left[\sum_j \frac{1}{\sqrt{(R_{1j}^{AB})^2 + \bar{d}^2}} + 2\pi\sigma\bar{d} \right] - \frac{\pi\sigma e^2}{\varepsilon} \bar{d}, \text{ etc.}$$

The regularized sums (like the one in the square bracket) vanish in the large-distance limit. Interestingly, they are amenable to a special representation by quickly converging series expansions, with the aid of the recent method developed in [18,19]. Note that the regularization of image interactions u_{im} requires addition and subtraction of an infinite number of background energies. After performing the regularization of all lattice sums in (6), we end up with

$$\frac{E_{pp}}{N} = \frac{E_{pp}^*}{N} - \frac{\pi\sigma e^2}{\varepsilon} \bar{d} - \frac{4\pi\sigma e^2}{\varepsilon} \frac{\Delta}{(1-\Delta)^2} \bar{d}, \quad (7)$$

where the star means “regularized”.

ii) *Particle-surface charge interaction*: We now study the direct and image interactions of charged particles with the fixed surface charge densities on the walls. The surface charge $-\sigma e$ at $z = -d/2$ has one image $\Delta(-\sigma e)$ at the same $z = -d/2$ and a series of images $(1+\Delta)\Delta^{n-1}(-\sigma e)$ at $z = (-1)^n(2n-1)d/2$ ($n = 2, 3, \dots$). The surface charge $-\sigma e$ at $z = +d/2$ has one image $\Delta(-\sigma e)$ at the same $z = +d/2$ and a series of images $(1+\Delta)\Delta^{n-1}(-\sigma e)$ at $z = (-1)^{n-1}(2n-1)d/2$ ($n = 2, 3, \dots$). After simple algebra, the interaction energy of one particle of charge e with both surface charges $(-\sigma e)$ and their images takes the form

$$\frac{E_{ps}}{N} = \frac{2\pi\sigma e^2}{\varepsilon} \frac{(1+\Delta)^2}{(1-\Delta)^2} \bar{d}. \quad (8)$$

The same result is obtained, as it should be, when one computes the interaction energy of both surface charges $(-\sigma e)$ with one charge e and all its images.

iii) *Surface charge-surface charge interaction*: The energy per particle due to the direct and image interaction between surface charges turns out to be

$$\frac{E_{ss}}{N} = -\frac{\pi\sigma e^2}{\varepsilon} \frac{(1+\Delta)^2}{(1-\Delta)^2} \bar{d}. \quad (9)$$

Note that this value equals to $-1/2$ of E_{ps}/N defined by (8), in close analogy with the homogeneous $\Delta = 0$ case.

For the total energy $E = E_{pp} + E_{ps} + E_{ss}$, we get

$$\frac{E}{N} = \frac{E_{pp}^*}{N} + \frac{\pi\sigma e^2}{\varepsilon} (d - \bar{d}). \quad (10)$$

The infinite lattice sums in E_{pp}^*/N , which is the regularized version of (6), can be expressed as quickly converging series of the special functions [18,19]

$$z_\nu(x, y) = \int_0^{1/\pi} \frac{dt}{t^\nu} e^{-xt} e^{-y/t}, \quad y > 0, \quad (11)$$

which represent a generalization to two-layer problems of the so-called Misra functions [22] used in single-layer lattice summations [23]. The cutoff of the series at the 5th term corresponds to the precision of more than 17 decimal digits; we keep this cutoff in the present work. As concerns the number of counted images in the image Coulomb potential (4), we cut the series at $n=5$ as well; there exist various checks indicating that this cutoff preserves excellent accuracy of our results.

We do not assume that the inclusion of repulsive images will lead to the appearance of a new structure, different from those presented in fig. 2. The energy per particle of a structure has to be minimized with respect to all structure parameters. In comparison with the $\Delta=0$ case, the bilayer distance \bar{d} is an additional variational parameter. Among the five afore-mentioned structures, the one which provides the minimum of the energy E is chosen as stable.

The appearance of three, four or more layered structures cannot be, in principle, excluded. Other approaches, like Monte Carlo (MC) simulations, are more suitable for detecting such complicated structures. We only know that the case $\Delta=0$ and the two extreme limits $d \rightarrow 0$ (structure I) and $d \rightarrow \infty$ (structure V) for all $\Delta \in [0, 1]$ are treated correctly within our assumption:

- As soon as $\Delta > 0$, the stability along the z -axis of a particle inside structure I is influenced “positively” by image/self-image effects and “negatively” by the direct Coulomb interaction with all other particles. The image effects become stronger when the distance between walls d decreases; there always exists a finite distance d when the image force overwhelms the direct repulsion by other particles. This is why structure I is expected to be stable in a finite interval of d values, in contrast to the $\Delta=0$ case.
- In the opposite limit $d \rightarrow \infty$, our energy per particle (10) reduces to that of the hexagonal Wigner crystal with images for one-wall geometry. Indeed, in that limit, the following terms survive from the regularized version of (6): the sum $\sum_{j \neq 1} 1/R_{1j}^{AA}$, $\Delta/[\varepsilon(d-\bar{d})]$ from the $n=1$ term of $u_{\text{im}}(0; \bar{d}/2, \bar{d}/2)$ and

$$\frac{\Delta}{\varepsilon} \left[\sum_{j \neq 1} \frac{1}{\sqrt{(R_{1j}^{AA})^2 + (d-\bar{d})^2}} + 2\pi\sigma(d-\bar{d}) \right]$$

from the $n=1$ term of $\sum_{j \neq 1} u_{\text{im}}(R_{1j}^{AA}; \bar{d}/2, \bar{d}/2)$. Substituting these terms into eq. (10) and expressing everything in terms of the distance l of the hexagonal

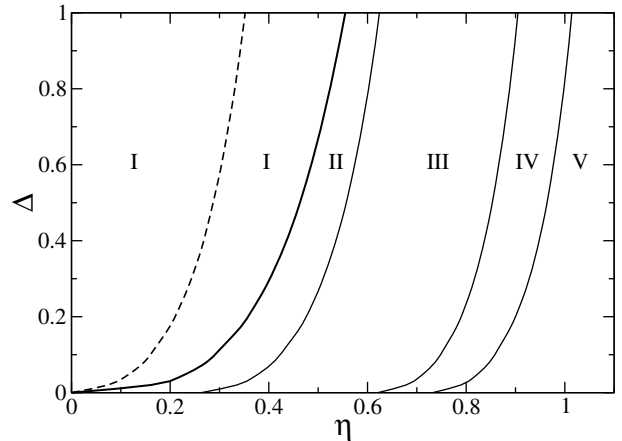


Fig. 3: The phase diagram in the (η, Δ) -plane. The dashed line, lying entirely in the structure-I region, corresponds to the absolute ground state (minimum of the total energy).

Wigner crystal from the wall, we recover the basic expression for the energy per particle (9) in [20] for the charge valence $q=1$. The two Wigner crystals form, together with the corresponding charged wall, neutral entities shifted as in structure V to ensure the lowest energy.

We shall work with dimensionless distances

$$\eta = d\sqrt{\sigma}, \quad \bar{\eta} = \bar{d}\sqrt{\sigma}, \quad \xi = l\sqrt{\sigma}, \quad (12)$$

such that $\xi = (\eta - \bar{\eta})/2$. In the asymptotic limit $\eta \rightarrow \infty$, the dimensionless distance of the Wigner layer from the corresponding wall is given by

$$\xi^* = \frac{t}{3^{1/4}\sqrt{2}} \quad (\eta \rightarrow \infty), \quad (13)$$

where t is the Δ -dependent solution of eqs. (1) and (2). This formula provides a check of the accuracy of our results in the region of structure V as well as criterion for reaching the asymptotic one-wall regime.

Numerical results. – We have performed numerical calculations using the Mathematica software. The phase diagram in the (η, Δ) -plane is pictured in fig. 3. Generally speaking, the transition values of η exhibit a much stronger dependence on Δ than the ones of $\bar{\eta}$ presented in table 1. The relevant fact is that for every $\Delta > 0$ the particles form the Wigner monolayer ($\bar{\eta}=0$) with structure I up to some positive $\eta_{\text{I} \rightarrow \text{II}} > 0$, as was anticipated.

Interestingly, for $\Delta > 0$ the ground-state energy is not a monotonic function of η . It reaches its global minimum at some η_{min} which is smaller than $\eta_{\text{I} \rightarrow \text{II}}$, *i.e.* the particles form the structure-I Wigner monolayer at this point, see fig. 4. Such a behavior differs substantially from the homogeneous case $\Delta=0$, for which the energy grows monotonically.

At point $\eta_{\text{I} \rightarrow \text{II}}$, the particle system starts to bifurcate to a Wigner bilayer ($\bar{\eta} > 0$) and at the same time structure

Table 1: The values of the dimensionless layer separation $\bar{\eta}$ at phase transitions between structures I \rightarrow II \rightarrow III \rightarrow IV \rightarrow V, for a given dielectric jump Δ .

Δ	$\bar{\eta}_{\text{I} \rightarrow \text{II}}$	$\bar{\eta}_{\text{II} \rightarrow \text{III}}$	$\bar{\eta}_{\text{III} \rightarrow \text{IV}}$	$\bar{\eta}_{\text{IV} \rightarrow \text{V}}$
0.2	0	0.273	0.619	0.732
0.4	0	0.267	0.607	0.723
0.6	0	0.259	0.596	0.712
0.8	0	0.252	0.587	0.703
1.0	0	0.245	0.578	0.693

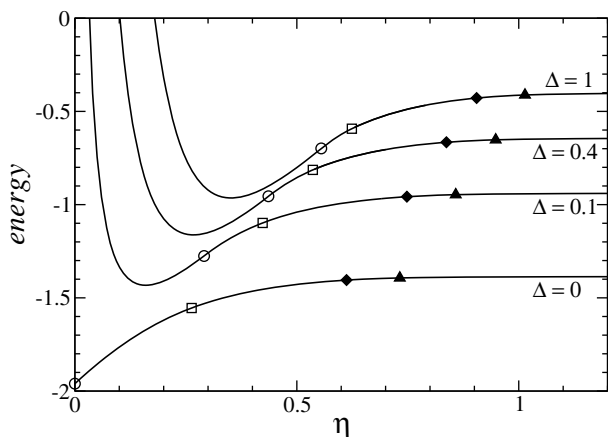


Fig. 4: The dimensionless ground-state energy per particle, $E\varepsilon/(Ne^2\sqrt{2\sigma})$, vs. the dimensionless distance between the walls η , for four values of the dielectric jump $\Delta = 0, 0.1, 0.4$ and 1. The symbols represent the transition points between structures: open circle for I \rightarrow II, open square for II \rightarrow III, filled diamond for III \rightarrow IV and filled triangle for IV \rightarrow V.

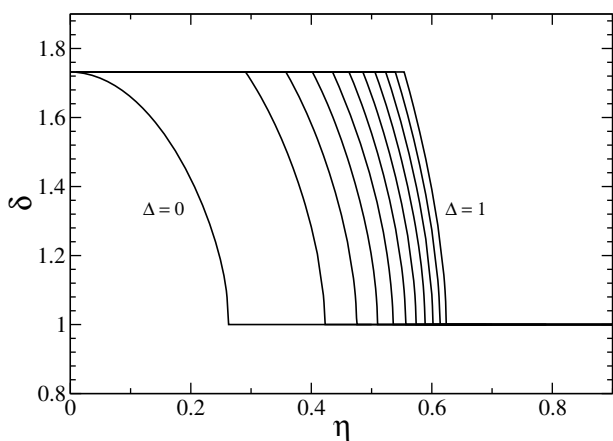


Fig. 5: The aspect ratio δ of structures I-III vs. the dimensionless distance between the walls η . The dielectric jump Δ ranges between 0 to 1, from left to right with step 0.1. $\delta = \sqrt{3} = 1.73205\dots$ for structure I, $1 < \delta < \sqrt{3}$ within structure II and $\delta = 1$ for structure III.

I evolves into structure II with the varying aspect ratio $1 < \delta < \sqrt{3}$ (see fig. 5). Structure II ends up at the second-order transition point $\eta_{\text{II} \rightarrow \text{III}}$, where structure III with

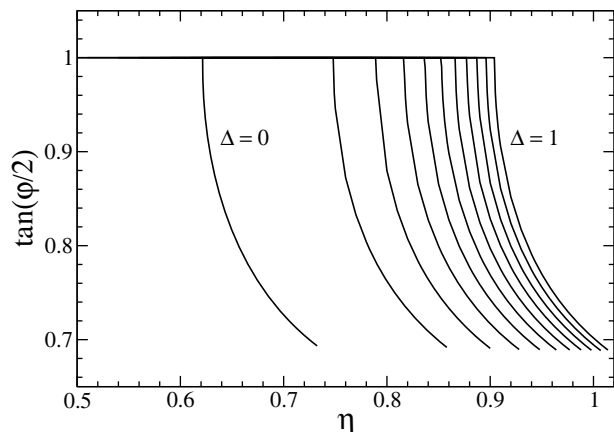


Fig. 6: Dependence of the angle φ for structure IV on the dimensionless distance between the walls η . The dielectric jump Δ ranges between 0 to 1, from left to right with step 0.1. Each line ends at the transition point $\eta_{\text{IV} \rightarrow \text{V}}$.

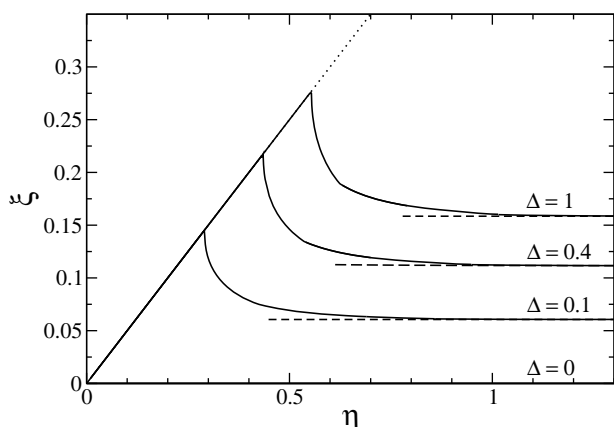


Fig. 7: Dimensionless distance of the Wigner sub-layer from the nearest wall, ξ , vs. the dimensionless distance between the walls η , for four values of the dielectric jump $\Delta = 0, 0.1, 0.4$ and 1. The dotted line has slope 1/2. For $\Delta = 0$, we have the trivial result $\xi = 0$, *i.e.* particles collapse onto the wall surface, as required by Earnshaw theorem. The horizontal dashed lines correspond to the asymptotic $\eta \rightarrow \infty$ values for the one-wall problem ξ^* , given by (13).

the fixed aspect ratio $\delta = 1$ determines the ground-state energy.

The second-order phase transition from structure III ($\varphi = \pi/2$) to structure IV, with a varying angle φ such that $\tan(\varphi/2) < 1$, takes place at point $\eta_{\text{III} \rightarrow \text{IV}}$. The plots of the order parameter $\tan(\varphi/2)$ vs. the dimensionless inter wall distance are pictured for the dielectric jumps $\Delta = 0, 0.1, \dots, 1$ in fig. 6.

At the first-order transition point $\eta_{\text{IV} \rightarrow \text{V}}$, the angle φ skips from the value ~ 1.21 within structure IV, which is practically independent of Δ , to $\pi/3 \sim 1.05$ for structure V. An interesting question is whether also the layer separation $\bar{\eta}$ exhibits a skip at $\eta_{\text{IV} \rightarrow \text{V}}$. The values of $\bar{\eta}_{\text{IV} \rightarrow \text{V}}$ for various Δ 's in the last column of table 1 turn out to be

the same for both structures IV and V at the transition point, within our number specification to 3 decimal digits.

In the last fig. 7, we plot the dimensionless distance of the Wigner sub-layer from the nearest wall, ξ , vs. η , for four values of the dielectric jump $\Delta \in [0, 1]$. The dielectric homogeneous case $\Delta = 0$ with the trivial $\xi = 0$, i.e. particle collapse onto the wall surface, is shown for comparison. For the corresponding transition points between the structures, see fig. 4. If $\Delta > 0$, the Wigner monolayer with structure I stays at $z = 0$ up to $\eta_{I \rightarrow II}$ and so $\xi = \eta/2$ for $0 \leq \eta < \eta_{I \rightarrow II}$. Interestingly, the value of ξ attained at $\eta_{I \rightarrow II}$ is always larger than the asymptotic $\eta \rightarrow \infty$ value ξ^* for the one-wall problem, given by eq. (13) and depicted by horizontal dashed lines in fig. 7. This is why, after bifurcation of the Wigner monolayer to the series of bilayer structures II-V by increasing η , the distance ξ goes to ξ^* from above. For $\eta \sim 1.3$, ξ coincides with the asymptotic value ξ^* to within 4 decimal digits.

Conclusion. – We have extended the standard study of the homogeneous dielectric version of the ground-state problem for particles with Coulomb pair interactions, constrained between two equivalently charged wall, to a more realistic inhomogeneous dielectric situation with repulsive electrostatic image charges. The analysis of the additional Coulomb lattice sums due to the images of particles and surface charges was performed. All lattice sums are treated within the recent method [18,19] which uses a bilayer generalization of Misra functions (11) to construct very quickly convergent series expansions for the ground-state energy. The numerical results obtained show that inclusion of repulsive images has two fundamental effects. Firstly, the particles do not collapse onto the charged surfaces of the walls, but create a Wigner monolayer or bilayer symmetrically with a nonzero spacing from the walls. The Wigner monolayer with the hexagonal structure I remains stable up to a certain (dimensionless) distance between the walls $\eta_{I \rightarrow II}$, where it starts to bifurcate into the series of bilayer structures II-V. Secondly, the ground-state energy exhibits as the function of the distance between the walls a minimum at some η_{\min} lying in the region of the structure-I Wigner monolayer.

Although thermal fluctuations are supposed to destroy a classical Wigner crystal at very low temperatures, their fingerprints persist within a recent strong-coupling theory [24] to higher (room) temperatures, in agreement with MC simulations. Based on the present work, we plan to extend that strong-coupling study by including wall images.

LŠ is grateful to LPTMS for its hospitality. The support received from Grants VEGA No. 2/0049/12 and CE-SAS QUTE is acknowledged.

REFERENCES

- [1] MANOHARAN H. C., SUEN Y. W., SANTOS M. B. and SHAYEGAN M., *Phys. Rev. Lett.*, **77** (1996) 1813.
- [2] TUTUC E., SHAYEGAN M. and HUSE D. A., *Phys. Rev. Lett.*, **93** (2004) 036802.
- [3] EISENSTEIN J. P. and MACDONALD A. H., *Nature*, **432** (2004) 691.
- [4] IMAMURA H., MAKSYM P. A. and AOKI H., *Phys. Rev. B*, **53** (1996) 12613.
- [5] TENG L. and TU L. I. P., *Phys. Rev. Lett.*, **90** (2003) 245004.
- [6] NESER S., BECHINGER C., LEIDERER P. and PALBERG T., *Phys. Rev. Lett.*, **79** (1997) 2348.
- [7] FALKO V. I., *Phys. Rev. B*, **49** (1994) 7774.
- [8] ESFARJANI K. and KAWAZOE Y., *J. Phys.: Condens. Matter*, **7** (1995) 7217.
- [9] GOLDONI G. and PEETERS F. M., *Phys. Rev. B*, **53** (1996) 4591.
- [10] MESSINA R. and LÖWEN H., *Phys. Rev. Lett.*, **91** (2003) 146101.
- [11] OĞUZ E. C., MESSINA R. and LÖWEN H., *EPL*, **86** (2009) 28002.
- [12] LOBASKIN V. and NETZ R. R., *EPL*, **77** (2007) 38003.
- [13] SCHWEIGERT I. V., SCHWEIGERT V. A. and PEETERS F. M., *Phys. Rev. Lett.*, **82** (1999) 5293.
- [14] SCHWEIGERT I. V., SCHWEIGERT V. A. and PEETERS F. M., *Phys. Rev. B*, **60** (1999) 14665.
- [15] WEIS J. J., LEVESQUE D. and JORGE S., *Phys. Rev. B*, **63** (2001) 045308.
- [16] MAZARS M., *Phys. Rep.*, **500** (2011) 43.
- [17] EARNSHAW S., *Trans. Cambridge Philos. Soc.*, **7** (1942) 97.
- [18] ŠAMAJ L. and TRIZAC E., *EPL*, **98** (2012) 36004.
- [19] ŠAMAJ L. and TRIZAC E., *Phys. Rev. B*, **85** (2012) 205131.
- [20] ŠAMAJ L. and TRIZAC E., *Contrib. Plasma Phys.*, **52** (2012) 53.
- [21] JACKSON J. D., *Classical Electrodynamics*, 3rd edition (Wiley, New York) 1998.
- [22] BORN M. and MISRA R. D., *Proc. Camb. Philos. Soc.*, **36** (1940) 466.
- [23] BOWICK M. J., CACCIUTO A., NELSON D. R. and TRAVESSET A., *Phys. Rev. B*, **73** (2006) 024115.
- [24] ŠAMAJ L. and TRIZAC E., *Phys. Rev. Lett.*, **106** (2011) 078301.